Distorted-wave impulse approximation and coupled-channels analysis of inelastic pion scattering from ^{18}O

S. Chakravarti,* D. Dehnhard, M. A. Franey, S. J. Seestrom-Morris,† D. B. Holtkamp,† C. L. Blilie,‡ and A. C. Hayes
School of Physics and Astronomy, University of Minnesota, Minneapolis, Minnesota 55455

C. L. Morris
Los Alamos National Laboratory, Los Alamos, New Mexico 87545

D. J. Millener
Brookhaven National Laboratory, Upton, New York 11973
(Received 4 March 1987)

Data for inelastic pion scattering from ^{18}O at $T_\pi = 164$ MeV, exciting the lowest 2^+, 3^-, and 1^- states, were analyzed by distorted-wave impulse approximation and coupled-channel calculations using transition densities derived from shell model calculations. Coupled-channels effects were found to be relatively unimportant for the 2^+ and 3^- states, but non-negligible for the excitation of the 1^- state. Nevertheless, the inclusion of multistep excitation paths is not sufficient to generate a fit to the 1^- data with the shell model wave functions. Major modifications are needed in the radial dependence of the neutron and proton parts of the transition density for the $0^+ \rightarrow 1^-$ one-step process.

I. INTRODUCTION

Inelastic pion scattering has been used successfully in determining the neutron-proton or, equivalently, the isospin composition of nuclear excitations (see Refs. 1–6, for example). Predictions based on microscopic structure models[1,2,7,8] have been tested and, in general, found to be in good agreement with the results of inelastic pion scattering experiments. Enhancement factors[2,4,6,9] consistent with those deduced from electromagnetic measurements[10,11] were needed to fit collectively enhanced transitions. The pion data have provided new information on the neutron parts of these collective transitions complementary to the electric charge information which can be obtained (chiefly) from electromagnetic measurements.

In most analyses of inelastic pion scattering, multistep processes involving intermediate excited states have been neglected. The validity of this approximation is questionable for weakly excited states, especially if they can be reached via intermediate states connected by strong, collectively enhanced transitions. A notable example is the transition to the first excited 1^- state in ^{18}O (4.46 MeV). The direct path is expected to be relatively weak and to be dominated by proton particle-hole components.[8] But there are two low-lying collective states,[12] 2^+(1.98 MeV) and 3^-(5.09 MeV), for which the calculations described in this paper predict large transition matrix elements[7] to the 1^- state. Thus multistep processes via both of these two states may be important.

Pion scattering on ^{18}O to the 1^- state showed two surprises which have been reported previously.[6,13] Firstly, at energies near the [3,3] pion-nucleon resonance, where a pure proton excitation is expected to be observed 9 times more strongly by π^+ than π^-, the experimental cross section ratio $\sigma(\pi^+)/\sigma(\pi^-)$ was found to be only slightly larger than 1. Secondly, theoretical calculations using the distorted wave impulse approximation (DWIA) and shell model transition densities[7] underestimate the experimental π^+ and π^- differential cross sections by large factors. The theoretical $B(E1) = 2.25 \times 10^{-5}$ W.u., however, is larger than the experimental upper limit[14] ($< 3 \times 10^{-6}$ W.u.).

It is possible that the (π,π') data could be reproduced by including multistep processes in the DWIA calculations. For collectively enhanced transitions in ^{24}Mg and ^{28}Si such coupled channels (CC) effects have been found[15] to be quite small in pion scattering. Similarly, CC effects were only partially successful[16] in removing the discrepancy between experiment and theory for the $^{13}C(\pi^+,\pi^0)$ reaction. However, in an analysis[17] of the weak transition to the first excited 0^+ state in ^{12}C, inclusion of a two-step path via the first excited 2^+ state was shown to improve the fit to the data significantly.

In this paper we present a DWIA and CC analysis of the (π,π') data for the first excited 1^- state in ^{18}O (4.46 MeV). Couplings between four low-lying states ($0^+,2^+,1^-,3^-$) were calculated using a momentum space, coupled channels computer program[16] developed by one of us (S.C.). A consistent set of shell-model transition densities was used for the transitions to the excited states and between the excited states. Effective charge enhancement factors were used which reproduce form factors from electron scattering and electromagnetic transition rates within this model.

For the direct $0^+ \rightarrow 1^-$ transition, the shell model transition density provides only a poor description of the electron scattering form factors (See III B 3 C). Thus, for the pion calculations we used both the bare shell model densi-

ty and one which we modified to reproduce the electron scattering data. We note that the shell model has difficulty predicting $E1$ electromagnetic transitions reliably because such transitions are generally hindered and subject to delicate cancellation effects.[18] The inelastic cross sections are relatively large in spite of the small size of the $E1$ transition density.[14] This means that $\Delta J=1$ densities other than electric dipole dominate the 1^- transition at the momentum transfers probed by inelastic scattering.

The paper is organized as follows. Section II contains a brief description of the experiment. In Sec. III we present the DWIA analysis using the transition densities derived from the shell model calculations and compare the results with our experimental data. Section IV is devoted to a description of the coupled-channels model used to study the effect of multistep processes in the excitation of the 1^- state, followed by a discussion of the results obtained using several different level-coupling schemes. In Sec. V we present a summary.

II. THE EXPERIMENT

The Energetic Pion Channel and Spectrometer[19] (EPICS) at the Clinton P. Anderson Meson Physics Facility (LAMPF) was used to take spectra for inelastic scattering of π^+ and π^- from ^{18}O. An oxygen gas target cooled to a temperature of 120 K was used at a pressure of 2 atm. The oxygen gas was enriched to 94.9% in ^{18}O. Spectra were taken for π^+ and π^- between 18° and 74° (c.m.) at $T_\pi=164$ MeV. Absolute differential cross sections were determined by measuring π-hydrogen scattering yields from a CH_4 gas target and extracting an overall normalization factor by comparing the π-p yields to predicted cross sections using the phase-shift values of Ref. 20. Further experimental details and typical spectra are discussed elsewhere.[4,21]

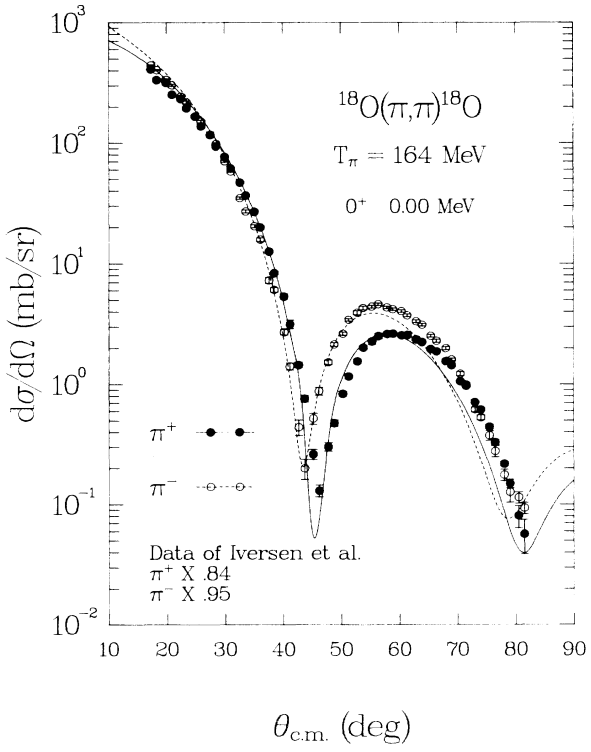

FIG. 1. Differential cross sections for π^+ and π^- elastic scattering from ^{18}O at $T_\pi=164$ MeV (data of Ref. 22 renormalized by a factor of 0.84 for π^+ and 0.95 for π^-). The solid and dashed lines were calculated with PIPIT using a g.s. density derived from electron scattering.

The error in the absolute cross sections is estimated as $\pm 8\%$ in addition to the statistical and background subtraction errors which are shown in the figures. In this paper we present only the data for the lowest 2^+, 3^-, and 1^- states. Data for other states will appear in another publication.[21] Our inelastic data are systematically lower than those of Iversen *et al.*[22] at forward angles where the latter experiment suffered from larger background and poorer resolution than the present experiment. For the first 2^+ state our value for the ratio $\sigma(\pi^-)/\sigma(\pi^+)=2.1\pm 0.2$ is within about one standard deviation of the value 1.86 ± 0.16 quoted in Ref. 22.

Our elastic data are lower than the earlier data[22] as well. We have used the more extensive elastic data of Ref. 22, after renormalization to our data by factors of 0.84 for π^+ and 0.95 for π^-, for comparison with optical model predictions (Fig. 1). The agreement with the optical model calculations is better for the renormalized data than the original data, except at the far forward angles ($\theta_{c.m.}\leq 25°$).

III. DWIA ANALYSIS

A. Elastic scattering

The momentum space elastic scattering code PIPIT (Ref. 23) was used to calculate the elastic scattering cross sections and to provide the distorted wave functions for the inelastic calculations with the code ARPIN.[1] For the off-shell extrapolation of the pion-nucleon amplitudes we used the phenomenological Gaussian cutoff model[23] with $a_l=3\times 10^{-6}$ MeV^2 for both the $l=0$ and 1 partial waves. For a better fit to the elastic data the pion-nucleon t matrix was calculated 16 MeV below the actual incident pion energy in the c.m. system. We note that in an analysis of the same data[21] with a coordinate-space code the required energy shift was 28 MeV.

For use in the calculations with PIPIT we deduced the ground state (g.s.) proton point density from the experimental charge density for electron scattering[24] by unfolding the finite charge distribution of the proton using the program ALLWORLD.[25] The neutron point density was obtained by simple N/Z scaling. The calculated DWIA curves with this g.s. density are shown in Fig. 1 and also in Fig. 2, solid line. When a three-parameter Fermi distribution, fitted to the electron data, was used, we found only small differences at forward angles ($\theta<90°$) but quite significant differences at backward angles near 180° (Fig. 2, dashed line).

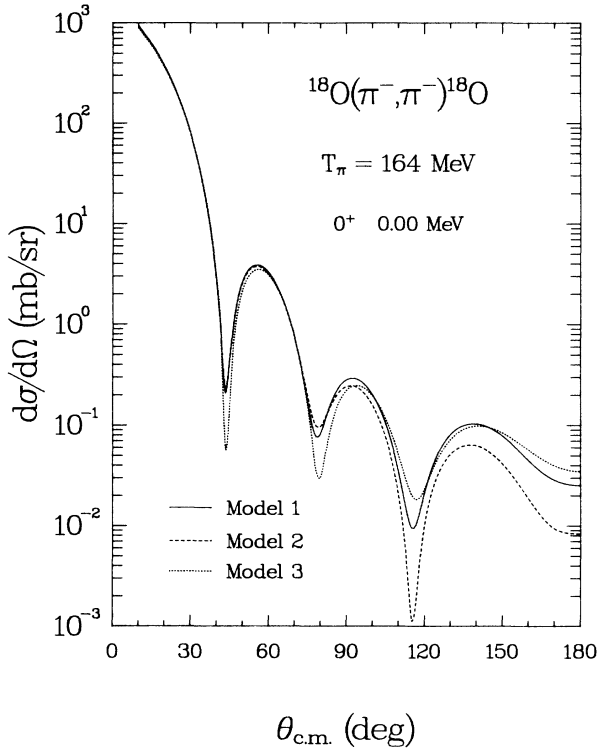

FIG. 2. Optical model and CC predictions for $^{18}O + \pi^-$ elastic scattering up to 180°. Solid line: with proton point density $\rho_p(r)$ derived from experimental charge distribution (Ref. 24, Table IX). Dashed line: with $\rho_p(r)$ from three-parameter Fermi representation (Ref. 24). Dotted line: CC calculation for coupling with the 2_1^+ and 3_1^- states using $\rho_p(r)$ as for the solid line.

B. Inelastic scattering

1. General remarks, transition densities

The transition densities needed in the DWIA and CC calculations were constructed using one-body density matrix elements (OBDME's), obtained from a shell model calculation done by one of us (D.J.M.) using the Chung-Wildenthal (CW) interaction[26] for the *sd* shell and the Millener-Kurath (MK) interaction[7] for all cross-shell matrix elements. The OBDME's are the reduced matrix elements of coupled creation and annihilation operators and the transformation between the *jj* and *LS* or SU3 coupling schemes can be simply performed (see Appendix). Our definition of the OBDME's differs from that of Lee and Kurath[1] only in the inclusion of an i^l factor with the spherical harmonic in the single particle wave function. We present the OBDME's in the SU3 version of *LS* coupling, which clearly exhibits the spin transfer $\Delta S=0$ or 1 to the target. Also, for the 0^+ to 1^- transition one SU3 amplitude dominates while another is constrained to be very small (subsection B 3 c).

For the positive parity states we used simple $(sd)^2$ wave functions ($0\hbar\omega$ model space). However, we also discuss the effect of using wave functions obtained with an expanded $(0+2)\hbar\omega$ model space (subsection B 2). In the case of the negative parity states, we employed the complete $1\hbar\omega$ space of $p^{-1}(sd)^3$ plus $(sd)^1(pf)^1$ configurations. Results pertinent to the excitation of the 1^- and 3^- levels are discussed in subsection B 3.

As is well known, the shell model densities do not reproduce the strength of collectively enhanced transitions as for the $0^+ \rightarrow 2^+$ (1.98 MeV) quadrupole and the $0^+ \rightarrow 3^-$ (5.09 MeV) octupole excitations. It is convenient to introduce polarization charges or enhancement factors[6,10,11] to account for the many small components in the wave functions which are not contained in a truncated shell model space. To minimize the number of adjustable parameters, we required that the polarization charges fit inelastic electron scattering data, electromagnetic transition rates, and the π^+/π^- cross section ratio as discussed below. In general, the components that core polarization add to the transition density will give rise to a q dependence which differs from that of the model space form factor. However, for collective transitions, with surface-peaked transition densities, constant polarization charges work well in practice, particularly if small adjustments in the oscillator parameter are made to optimize the fit to the shape of the measured (e,e') cross sections.

The longitudinal ($\Delta S=0$) form factor from (e,e') determines the proton part, $\rho_p'(r)$, of the transition density. This experimental transition density can be expressed in terms of the proton, $\rho_p(r)$, and neutron, $\rho_n(r)$, parts predicted by the shell model, using polarization charges, i.e.,

$$\rho_p'(r)=(1+\delta_p^p)\rho_p(r)+\delta_p^n\rho_n(r) \ . \tag{1}$$

Here, δ_p^p (δ_p^n) parametrizes the extent to which the "valence" protons (neutrons) polarize the proton core. Electron scattering provides us with a relation between δ_p^p and δ_p^n.

Pion scattering involves not only the proton part $\rho_p'(r)$ of the transition density, but also its neutron part, $\rho_n'(r)$, which is written similarly to Eq. (1) as

$$\rho_n'(r)=(1+\delta_n^n)\rho_n(r)+\delta_n^p\rho_p(r) \ . \tag{2}$$

Here, δ_n^n (δ_n^p) parametrizes the polarization of the core neutrons by the "valence" neutrons (protons). The enhanced transition densities can also be written, using the isospin formalism, in terms of the shell model isoscalar and isovector densities,

$$\rho_0(r)=\tfrac{1}{2}[\rho_n(r)+\rho_p(r)]$$

and

$$\rho_1(r)=\tfrac{1}{2}[\rho_n(r)-\rho_p(r)] \ ,$$

respectively, i.e.,

$$\rho_0'(r)=(1+\delta_0)\rho_0(r)$$

and (3)

$$\rho_1'(r)=(1+\delta_1)\rho_1(r) \ .$$

Here, δ_0 and δ_1 are the isoscalar and isovector polarization charges. Since the core contains the same number of neu-

trons as protons, we set $\delta_n^n=\delta_p^p$ and $\delta_n^p=\delta_p^n$ as in Ref. 11. This leads to

$$\delta_0=\delta_n^n+\delta_n^p=\delta_p^p+\delta_p^n$$

and (4)

$$\delta_1=\delta_n^n-\delta_n^p=\delta_p^p-\delta_p^n$$

or, equivalently,

$$\delta_n^n=\delta_p^p=\tfrac{1}{2}(\delta_0+\delta_1)$$

and (5)

$$\delta_n^p=\delta_p^n=\tfrac{1}{2}(\delta_0-\delta_1)\ .$$

The longitudinal form factor from (e,e') is proportional to $[\rho_0'(r)-\rho_1'(r)]$ and thus yields a constraining relationship between δ_0 and δ_1.

For [3,3] resonance dominance and in the plane wave impulse approximation, the differential cross sections for inelastic pion scattering are given by[2]

$$\sigma(\pi^+)\propto[3\rho_p'+\rho_n'(r)]^2\propto[2\rho_0'(r)-\rho_1'(r)]^2$$
$$\sigma(\pi^-)\propto[3\rho_n'(r)+\rho_p'(r)]^2\propto[2\rho_0'(r)+\rho_1'(r)]^2\ . \quad (6)$$

Thus, π^+ and π^- scattering provide us with two more relations between δ_0 and δ_1.

At present, DWIA predictions of absolute differential cross sections for inelastic pion scattering are believed to have a $\pm 20\%$ uncertainty. However, the π^+/π^- cross section ratio can be predicted much more reliably. Thus we decided to use the (e,e') form factor and the π^+/π^- ratio to determine δ_0 and δ_1. We also required consistency with experimental electromagnetic transition rates.

We calculated the $\rho_0(r)$ and $\rho_1(r)$ using the shell model OBDME's and harmonic oscillator (HO) wave functions and adjusted δ_0 and δ_1 to reproduce the π^+/π^- ratio and the (e,e') form factors at 90° (which are dominated by the $\Delta S=0$ part of the transition density). We found that, in order to fit the shapes of the form factors, it was necessary to use values of the oscillator parameter b different from the ground state value calculated from the experimental rms charge radius of ^{18}O, $\langle r_{ch}^2\rangle^{1/2}$.

In plane wave calculations for electron scattering it is customary to explicitly include a center of mass correction. An oscillator parameter b' is obtained from

$$\langle r_{ch}^2\rangle-\langle r_p^2\rangle=b'^2\left\{\sum_Q\left[Q\frac{z(Q)}{Z}\right]+\frac{A-1}{A}\frac{3}{2}\right\}, \quad (7)$$

and the shell model form factors $F(q)$ in momentum space are multiplied by the factor $e^{b'^2q^2/4A}$ before comparison with the experimental data. Here, q is the momentum transfer and A is the target mass, and $z(Q)$ is the number of protons in the major shell with $Q=2n+l$ oscillator quanta where $n\geq 0$, i.e., $z(Q=0)=2$ for the full $0s$ shell and $z(Q=1)=6$ for the full $0p$ shell. Z is the total number of protons and $\langle r_p^2\rangle^{1/2}$ is the rms charge radius of the proton. Using the value $\langle r_{ch}^2\rangle^{1/2}=2.784$ fm (Ref. 12) and $\langle r_p^2\rangle^{1/2}=0.80$ fm, Eq. (7) gives $b'=1.812$ fm. This oscillator parameter is appropriate for single particle wave functions in which the radial coordinate is referred to the origin of the shell-model potential.

In distorted wave codes, however, nucleon coordinates are measured relative to the center of mass of the nucleus (A) and, because of the distortion, the center of mass correction cannot be made to the observables (i.e., the angular distributions) explicitly. For harmonic oscillator wave functions the transformation from r_i (measured relative to the origin) to $r_{i,A}$ (measured relative to the center of mass of the nucleus) can be made (Ref. 18). The transition density is then a function of the coordinate $r_{i,A}$ with the radial scale defined by

$$b=\left[\frac{A-1}{A}\right]^{1/2}b'\ . \quad (8)$$

If the electron scattering data are fitted in the plane wave Born approximation with no explicit center of mass correction, then the parameters b, δ_0, and δ_1 describe the physical transition density as a function of $r_{i,A}$. In principle,[18] the standard shell-model OBDME's are modified by the coordinate transformation from r_i to $r_{i,A}$, but in this work these changes are insignificant compared to the large changes in the shell model transition densities necessary to fit the (e,e') and (π,π') data. The value $b'=1.812$ fm corresponds to $b=1.761$ fm. A more recent value, $\langle r_{ch}^2\rangle^{1/2}=2.801$ fm (Ref. 24), gives a slightly larger value of $b=1.772$ fm. The best fit values of b for the inelastic form factors were $b=1.70$ fm for the 2^+ state and $b=1.80$ fm for the 3^- state (see below). Unless explicitly stated, we use the phenomenological values of b and therefore our transition densities are properly used without center of mass corrections.

By our method of adjusting b, δ_0, and δ_1, we generate semiphenomenological transition densities for $\Delta S=0$ (in a harmonic oscillator representation using shell model OBDME's) which can be used directly in the DWIA calculation for (π,π') with the code ARPIN.[1] For the $\Delta S=1$ part of the transition densities, we used the transition density amplitude predicted by the shell model without enhancement or quenching, but with the adjusted values of b.

2. *Transition to the 2^+ state (1.98 MeV)*

For the (π,π') calculations in this work we used shell model predictions for which the ground state (g.s.) of ^{18}O was assumed to be a pure two-particle–zero-hole (2p-0h) state. Without polarization charges this model implies a pure neutron excitation for the 2^+ state for which $\sigma(\pi^-)/\sigma(\pi^+)\simeq 9.0$ and $B(E2)=0$. However, the experimental π^-/π^+ ratio is only 2.1 ± 0.2 and the $B(E2)$ is quite large. We found a good fit to the (e,e') data[24] using the plane wave (e,e') program ELEC,[27] with $b=1.70$ fm and $\delta_p^n=\delta_n^n=0.8$ (i.e., $\delta_0=1.6$ and $\delta_1=0$). The pion ratio $\sigma(\pi^-)/\sigma(\pi^+)=2.1$ for this state is fitted best in a DWIA calculation with $\delta_n^n=\delta_p^n=0.7$ and the experimental[28] $B(E2\uparrow)=(47.6\pm 1.0)\ e^2\text{fm}^4$ is reproduced with $\delta_p^n=0.83\pm 0.01$ if $b=1.70$ fm. We decided to use an average of $\delta_n^n=\delta_p^n=0.75$ with $b=1.70$ fm for all subsequent DWIA and CC calculations involving $E2$ transitions. There was no compelling reason to make δ_n^n different from δ_p^n for this transition; thus, only the isoscalar spin-

independent part of the shell model transition density was enhanced by a factor $1+\delta_0=2.5$, and the isovector and the spin-dependent transition densities were left unchanged. The absolute differential cross sections calculated in the DWIA with these enhancement factors are slightly larger than the data (Fig. 3). Use of $\delta_n^n=\delta_p^n=0.7$ would fit the cross sections better, but the differences are smaller than the $\pm 20\%$ uncertainly in the DWIA. Thus we made no attempt to adjust the polarization charges further.

We note that smaller polarization charges ($\delta_n^n=\delta_p^n=0.58$) are needed to fit the (e,e') form factor for the $0^+\rightarrow 2_1^+$ transition with $b=1.7$ fm when $2\hbar\omega$ configurations, principally 4p-2h, are included in the model space as outlined in Ref. 29. The intensities of the $2\hbar\omega$ components in the 0_1^+ and 2_1^+ in the wave functions are 10% and 18%, respectively. In this case the effective charges are much closer to those employed[24] to fit the $d\rightarrow d$ and $d\rightarrow s$ transitions in ^{17}O. Because the transition densities between the excited states (which are required for the CC calculations) were obtained with the smaller shell model space, we used the simpler $0\hbar\omega$ densities also for the $0^+\rightarrow 2_1^+$ transition in the (π,π') calculations.

3. *Transitions to negative parity states*

a. General discussion of the negative parity wave functions. In the weak-coupling model calculation[8] of Ellis and Engeland (EE) the dominant components in the wave functions of the lowest 1^- and 3^- levels arise from the coupling of a $p_{1/2}$ proton hole to the $\frac{1}{2}^+$ (94%) and $\frac{5}{2}^+$ (96%) members, respectively, of the ^{19}F $(sd)^3_{T=1/2}$ ground state band. In the full $1\hbar\omega$ calculation with the MK interaction, these are still the dominant components at 76% and 67%, respectively. However, as can be seen from Table I, it is clearly an inadequate approximation to include $(sd)^3$ configurations with only $T=\frac{1}{2}$ which allow only pure proton excitations.

When the single-particle energies used in the shell-model calculation are taken from $A=15$ and 17, the lowest 1^- level is underbound by about 1 MeV, in agreement with the EE results.[8] If the theoretical spectrum is shifted to reproduce the excitation energy of the 1_1^- level (4.46 MeV), there is good agreement with the experimental level scheme (including the unnatural parity levels not shown in Table I), except for a slight compression which is reminiscent of the results of a similar calculation[4] for ^{17}O. It is noteworthy that most states show large admixtures (Table I) of configurations in which the three particles in the sd shell are coupled to $T=\frac{3}{2}$. The presence of $|p^{-1}\times(sd)^3_{T=3/2}\rangle$ wave function components means that both neutron and proton $p\rightarrow sd$ amplitudes can contribute to inelastic excitations from an $(sd)^2$ ground state; in contrast, in the EE model only proton amplitudes contribute by construction. This feature is evident in Table I, where the OBDME's for an sd particle and a p hole coupled to $(\lambda\mu)=(21)$ SU3 symmetry and $\Delta S=0$ are given (see following sections).

b. Transition to the 3^- *state at 5.09 MeV.* The π^+/π^- ratio of nearly 1.0 for the first 3^- state at 5.09 MeV indicates a predominantly isoscalar (or isovector) transition in contrast to predictions of the EE model, where the transition proceeds by pure proton $p\rightarrow sd$ excitations. We note

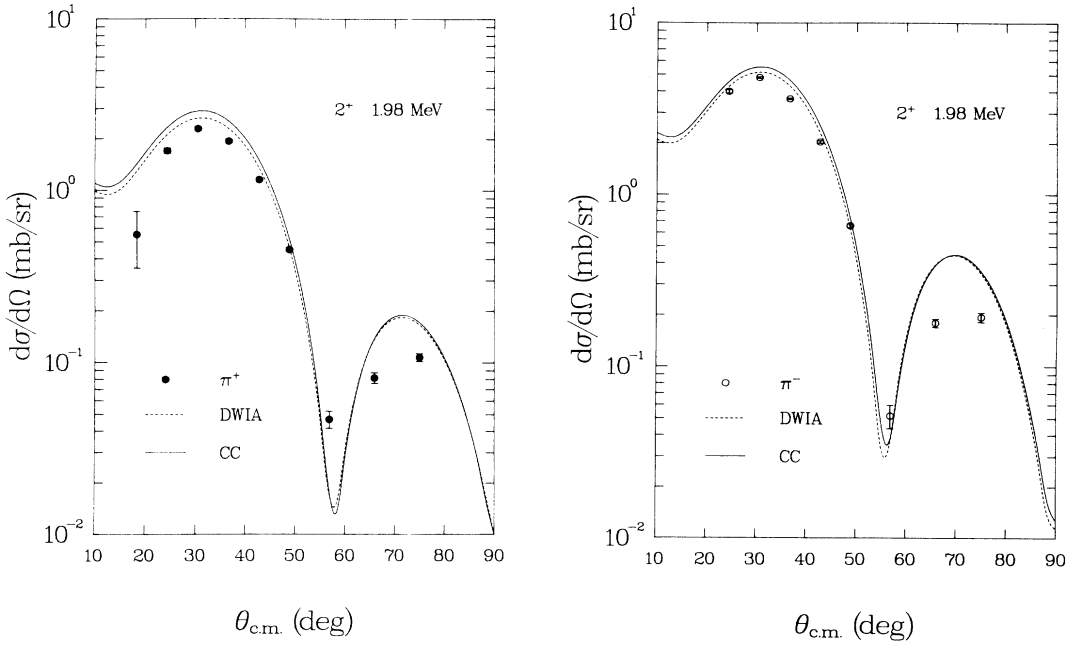

FIG. 3. Differential cross sections for ^{18}O$(\pi,\pi')^{18}$O$(2^+$, 1.98 MeV) at $T_\pi=164$ MeV (Ref. 21 and this work). The dashed lines were calculated with ARPIN (Ref. 1) using enhanced shell model OBDME's and $b=1.70$ fm. The solid lines are the results of CC calculations (Sec. IV).

TABLE I. Negative parity wave functions for ^{18}O.

J_n^π	E_x(expt) (MeV)	E_x(theor) (MeV)	$[p^{-1}(sd)^3_{T=1/2}]$ (%)	$[p^{-1}(sd)^3_{T=3/2}]$ (%)	$[(sd)^1(pf)^1]$ (%)	Z_0[a]	Z_1[a]
1_1^-	4.46	4.46[b]	91.4	6.6	2.0	0.3561	−0.3066
1_2^-	6.20	6.92	54.0	30.1	15.9	0.3115	−0.0637
1_3^-	7.62	7.69	31.7	62.2	6.1	−0.5518	−0.1742
1_4^-	8.04	8.09	45.0	45.6	9.3	0.1030	0.1048
3_1^-	5.10	4.71	80.2	16.8	3.0	−0.6091	0.2074
3_2^-	6.40	6.19	31.6	68.0	0.4	−0.4242	−0.2276
5_1^-	7.86	7.24	60.9	37.2	1.9		
5_2^-	8.13	7.72	47.9	49.8	2.3		

[a]OBDME or Z coefficients for $(\lambda\mu)=(21)$, $\Delta S=0$, $\Delta L=J$. Subscripts refer to isospin transfer ΔT. The matrix elements are reduced with respect to spin but not isospin (Brink-Satchler definition, Ref. 30). Thus, with our isospin convention, Z_1 contains a factor $\sqrt{1/2}$ from the isospin Clebsch-Gordan coefficient so that $Z(\text{neutron/proton})=\sqrt{1/2}(Z_0\pm Z_1)$. For example, for the 1_1^- state the proton amplitude Z_p is 0.4686 and the neutron amplitude Z_n is 0.0350. The jj coupling OBDME's can be obtained using the equations given in the Appendix.

[b]E_x(theor) are shifted so that the lowest 1^- level coincides with the E_x(expt).

from Table I, however, that for the 3_1^- state the MK interaction gives rise to an isoscalar $p\rightarrow d$ ($\Delta L=3$, $\Delta S=0$) amplitude which is 3 times the corresponding isovector amplitude. (The SU3 label is redundant in this case.) Small $sd\rightarrow pf$ neutron amplitudes also make the longitudinal part of the octupole transition density ($C3$) more isoscalar. The isoscalar strength is expected to be further augmented by core polarization corrections. Since the $p\rightarrow d$ transition density is obviously surface peaked, it is to be expected that simple scaling of the transition density will give a reasonable fit to the 3^- form factor.

Nevertheless, to reproduce the experimental π^+/π^- ratio it was necessary to make the transition *purely* isoscalar (i.e., $\delta_1=-1.0$). Both the π^+/π^- ratio and the longitudinal form factor from (e,e′) were then fitted with $\delta_0=0.8$ and $b=1.80$ fm. These parameters predict $B(E3\uparrow)=1230\ e^2\text{fm}^6$, in good agreement with experiment,[31] $B(E3\uparrow)=1120\pm105\ e^2\text{fm}^6$.

We note that the octupole transitions in ^{17}O(π,π') have been reproduced quite well[4] with $\delta_0=1.2$, $\delta_1=0.0$, and $b=1.63$ fm using shell model predictions with the MK interaction as in this work. These parameters do not fit the π^+/π^+ ratio for ^{18}O(π,π') for the 3^- state. We also note that there is no experimental evidence[32] from (e,e′) for the large isovector $\Delta S=1$ components predicted by the shell model. Nevertheless, since these components contribute only relatively little to pion scattering, we left all $\Delta S=1$ pieces unchanged from the shell model values. Using $\delta_0=0.8$ and $\delta_1=-1.0$ for the $\Delta S=0$ pieces, we found that the DWIA predictions for the absolute cross sections are below the experimental data by about a factor of 1.3 for π^+ and 1.6 for π^-.

Clearly, the modifications of the shell model transition densities which are needed to fit the 2^+ and 3^- data are quite severe and indicate a significant shortcoming in the model space. However, once $2\hbar\omega$ components are included in the calculation for the positive parity states, the required effective charges drop to values roughly consistent with those which are needed to reproduce enhanced $E2$ transition strengths over a wide range of nuclei. This use of an effective one-body operator is by far the most economical way to include core polarization effects predominantly associated with the excitation of a single nucleon through two major shells. For use in inelastic scattering the q dependence of the effective single-particle matrix elements should differ from that of the pure single particle matrix elements. A phenomenological example of this approach is pursued in Ref. 24.

For the 3^- state, the DWIA curves (Fig. 4) indicate a need for larger effective charges ($\delta_0=1.2$) than deduced from (e,e′). In Sec. IV we discuss whether CC effects are responsible for some of the difficulties which we encountered in using the shell model OBDME's.

c. Transition to the 1^- state at 4.46 MeV. It is worthwhile to begin with a general discussion of the properties of $C1$ transition densities ($\Delta L=1$, $\Delta S=0$) in light nuclei. We concentrate on the $p\rightarrow sd$ amplitudes, of which there are two with $\Delta L=1$, $\Delta S=0$; namely, $0p\rightarrow 1s$ and $0p\rightarrow 0d$. In the $1\hbar\omega$ model there are very strong constraints on the shape of the $C1$ form factor, and to make this clear it is convenient to use the SU3 basis. The amplitudes for $(\lambda\mu)$ equal to (10) and (21) are expressed in terms of the $(p\rightarrow s)$ and $(p\rightarrow d)$, 1p-1h OBDME's (in LS coupling) by the linear combinations

$$\begin{aligned}(10):&\ -\sqrt{1/6}(p\rightarrow s)+\sqrt{5/6}(p\rightarrow d)\ ,\\ (21):&\ -\sqrt{5/6}(p\rightarrow s)-\sqrt{1/6}(p\rightarrow d)\ ,\end{aligned}\tag{9}$$

where the conventions for the single particle wave functions are $R_{nl}>0$ for $r\rightarrow 0$, $1+s\rightarrow j$, and i^l is included with Y_m^l. In an oscillator model the center of mass ($R_{\text{c.m.}}$) and $E1$ operators transform as $(\lambda\mu)=(10)$ under SU3 with $\Delta T=0$ and 1, respectively. By definition,

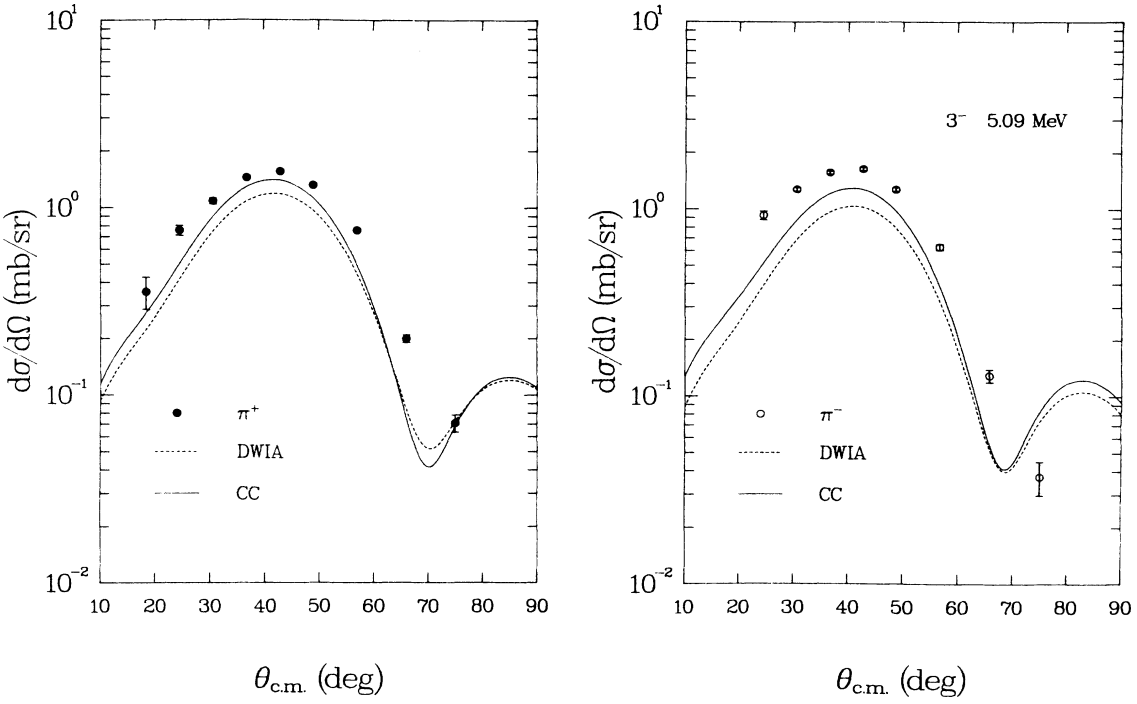

FIG. 4. Same as Fig. 3, but for the 3^- (5.09 MeV) state with $b=1.80$ fm.

$$\text{(i)}\ \langle f||R_{\text{c.m.}}||i\rangle=0\ . \tag{10}$$

For the low lying states,

$$\text{(ii)}\ \langle f||E1||i\rangle\simeq 0\ , \tag{11}$$

e.g., $B(E1)\leq 3\times 10^{-6}$ W.u. (Ref. 14) for ^{18}O(1^-; 4.46 MeV$\rightarrow$g.s.). The presence of $sd\rightarrow pf$ amplitudes ($0s\rightarrow 0p$ amplitudes for $A<16$) is important to ensure that (i) and (ii) are satisfied. We note that, in general, the $(\lambda\mu)=(10)$ amplitudes for different pairs of major shells are small for low-lying nuclear levels. This means that the longitudinal form factor F_L will generally be controlled by the $p\rightarrow sd$, $(\lambda\mu)=(21)$ amplitude. The model $C1$ form factor which is dominated by the $(\lambda\mu)=(21)$ amplitude has the same shape as a $C3$ form factor ($\Delta L=3$, $\Delta S=0$) with $F_L\sim y^{3/2}e^{-y}$, where $y=(bq/2)^2$. However, the experimental form factor for ^{18}O at 90° (Ref. 32) [and also for ^{16}O (Ref. 33)] is more narrow and peaked at a lower q than the model form factor calculated with $b'=1.812$ fm and center of mass correction (Fig. 5). Curve a in Fig. 5 shows the calculated total $|F_L|^2$; i.e., it includes a small $\Delta S=1$ contribution which does not improve the fit to the shape of the experimental form factor. In addition, the predicted $0\hbar\omega\rightarrow 1\hbar\omega$ form factors are too low in magnitude. Nevertheless, it is clear that contributions from the $(\lambda\mu)=(10)$ amplitudes must be small since the associated form factor is out of phase with the data (Fig. 5, curve c) and since the $B(E1)$ [and thus the $(\lambda\mu)=(10)$ amplitude] is known to be small from experiment.[14]

We note that the $p\rightarrow sd$, $(\lambda\mu)=(21)$ transition density displays qualitatively the behavior of the experimental ($0^+\rightarrow 1^-$) transition densities for ^{18}O and ^{16}O (Refs. 32 and 33, respectively); namely, a peaking in the interior with a sign change in the nuclear surface. The $(\lambda\mu)=(10)$ (giant-dipole) transition density is, in contrast, surface peaked. A further point to note is that the $(\lambda\mu)=(21)$ transition density, which involves mostly $p\rightarrow s$, is sensitive to the choice of single-particle wave function. For Woods-Saxon (WS) wave functions $|F_L|^2$ is narrowed somewhat, e.g., $|F_L|^2$ (WS) is a factor of 2 smaller than $|F_L|^2$ (HO) at $q=2.5$ fm^{-1}, although not enough to reproduce the data.

The experimental π^+/π^- cross section ratio is 1.3 ± 0.2 for the transition to the first 1^- state, in sharp contrast to the expected value of 9.0 for the pure proton transition[8] in the $0p\rightarrow 1s\,0d$ model. In the shell model calculation used here (which includes all possible $1\hbar\omega$ neutron excitations), the transition is still proton dominated (see Table I). Furthermore, early DWIA calculations[6] using the same shell model densities predicted π^+ and π^- cross sections smaller than the data by large factors. These discrepancies were the motivation for doing the CC calculation of the present work. When the (e,e') data[32] became available for this state, it was clear that the shell model densities would not reproduce the (e,e') form factors either. Following the prescription described earlier, we fitted the π^+/π^- ratio and the (e,e') form factor at 90° (Fig. 5, curve b) with $\delta_0=2.5$, $\delta_1=-0.5$, and $b=2.05$ fm for the $\Delta S=0$ pieces.

Figure 6 shows the DWIA predictions and the pion data for the 1^- state. With the bare shell model transition densities and $b=1.812$ fm, the DWIA cross sections

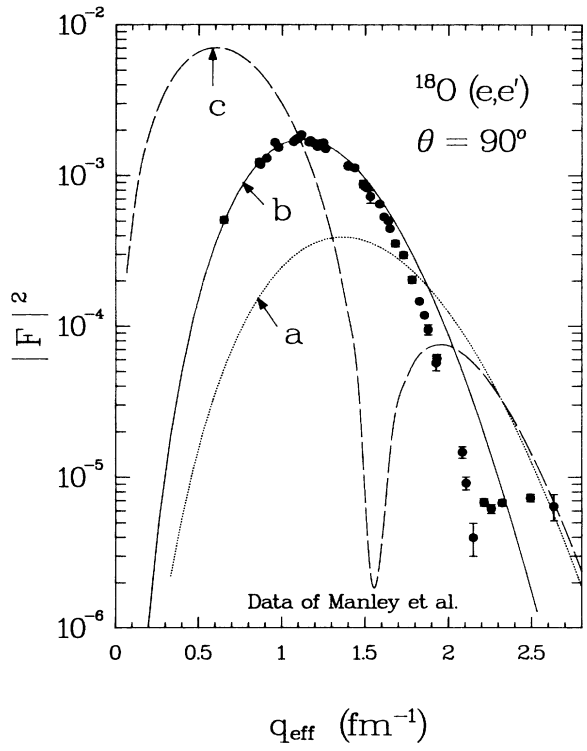

FIG. 5. Form factor for (e,e') scattering at $\theta=90°$ to the 1^- state in ^{18}O. The data are from Ref. 32. The dotted curve (a) is obtained from the bare shell model transition density for the 1^- state using $b'=1.812$ fm, and the solid curve (b) from the semiphenomenological transition density shown in Fig. 7. The long-dashed curve was obtained using a pure $(\lambda\mu)=(10)$, $T=1$ OBDME, which gives $B(E1)$ (1^- to 0^+)=1.77 W.u. for $b'=1.812$ fm. For a pure $(\lambda\mu)=(10)$, $T=1$ p-h state in ^{16}O one would get twice this value (from the isospin Clebsch-Gordan coefficient) modified by the A dependence of b and the W.u. This value would be the sum rule limit for a closed-shell ground state.

are a factor of 8 (25) smaller than the data for π^+ (π^-) and slightly out of phase with the experimental angular distributions (Fig. 6, left). Use of $b=1.761$ fm [Eq. (8)] would have been more appropriate here, but the difference between the DWIA cross sections for $b=1.812$ and 1.761 fm are insignificant in comparison with the large discrepancy between the DWIA prediction and the experiment.

We note that the shapes of the angular distributions are determined by the delicate interference of the $0p\rightarrow 1s$ and $0p\rightarrow 0d$ parts of the transition density. Single-component densities generate angular distribution shapes which are completely out of phase with the data. When the enhancements deduced from the (e,e') data and the π^+/π^- ratio are used ($1+\delta_0=3.5$ and $1+\delta_1=0.5$) with $b=2.05$ fm, the π^+ and π^- angular distributions are fitted perfectly both in shape and magnitude, except at the largest angle (Fig. 6, right).

The modification of the $\Delta S=0$ isoscalar shell model transition density for the 1^- state is even more drastic than for the 3^- state (preceding section). The harmonic oscillator parameter $b=2.05$ fm is unrealistically large when compared to $b=1.70$ fm (1.80) fm for the 2^+ (3^-) state transitions and to $b=1.761$ fm for the ground state density [Eqs. (8) and (7)]. However, the radial transition density generated with these parameters fits the (e,e') form factor at 90° between momentum transfers of $q=0.7$ and 1.8 fm^{-1}. Thus, it must be a reasonable representation of the actual transition density. We hope that with a more physical value for b near 1.8 fm larger-space shell model calculations would generate transition densities similar to the semiphenomenological densities which we use here.

The bare shell model and the fitted spin-independent radial transitions densities $\rho_p(r)$, $\rho_n(r)$, $\rho'_p(r)$, and $\rho'_n(r)$ are shown in Fig. 7. $\rho_p(r)$ and $\rho_n(r)$ were obtained with $b=1.812$ fm and $\rho'_p(r)$ and $\rho'_n(r)$ were calculated with $b=2.05$ fm, $1+\delta_0=3.5$, and $1+\delta_1=0.5$ [i.e., the values which fit the (e,e') data and the π^+/π^- cross section ratio]. ρ'_p is similar in magnitude to ρ_p, but is stretched towards larger r because of the larger value of b. ρ'_n is strikingly different from ρ_n in magnitude and spin, and, of course, also stretched towards larger r. We note that electron scattering is sensitive only to $\rho'_p(r)$ (if $\Delta S=0$), but it samples $\rho'_p(r)$ at all r. Pion scattering is sensitive to both $\rho'_p(r)$ and $\rho'_n(r)$ but, because of strong absorption, samples the transition density only from about $r=3$ fm outward in this case. Thus the π^+ and π^- data determine the outer lobe of $\rho'_n(r)$, but provide little information on $\rho'_n(r)$ for $r\lesssim 3$ fm. Nevertheless, it seems clear that the shell model used here does not generate a realistic neutron transition density since it underestimates $\rho_n(r)$ significantly at large r ($r\gtrsim 3$ fm).

While it is probably necessary to go outside the present shell-model space to reproduce both the shape and the magnitude of the cross sections for inelastic excitation of the 4.46 MeV level in ^{18}O, it is interesting to see what improvements could come about within the restriction to $0\hbar\omega$ and $1\hbar\omega$ model spaces. The lowest 1^- model state has a large $[p_{1/2}^{-1}\times{}^{19}\text{F(g.s.)}]$ component and consequently exhausts most of the $p_{1/2}$ proton pickup strength. This is in disagreement with the results from the ^{19}F(d,^{3}He)^{18}O reaction,[34] which yields C^2S values for the 4.46, 6.20, and 7.76 MeV 1^- levels equal to 1.31, 0.70, and 0.42, respectively. If we ignore the possibility of $p_{3/2}$ pickup, which is predicted to be small to states at low excitation, the 2^- levels which are unresolved from the second and third 1^- levels, cannot contribute to the latter two C^2S values. In addition, the 1^- levels can now be reached only by $p_{1/2}$ pickup and it is clear[35] that the first three 1^- model states (Table I) have to be mixed to reproduce the pickup data. If we choose the amplitudes for the $|1_1^-\rangle$, $|1_2^-\rangle$, and $|1_3^-\rangle$ components in the lowest mixed state to be $\sqrt{2/3}$, $\sqrt{1/6}$, and $-\sqrt{1/6}$, respectively, the isoscalar $(\lambda\mu)=(21)$ amplitude in this state is strongly enhanced and the isovector amplitude considerably weakened. With these mixed 1^- wave functions the unenhanced DWIA cross sections are still a factor of 4.4 (3.9) smaller than the data for π^+ (π^-), but the predicted π^+/π^- ratio is 1.2, in

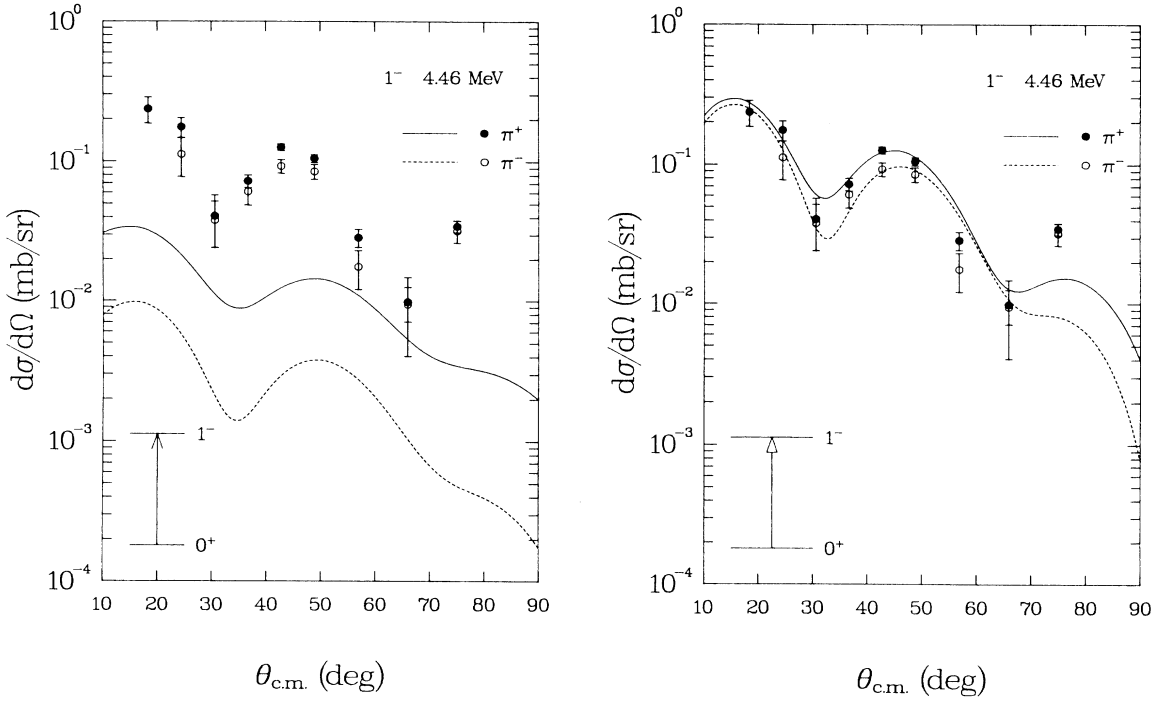

FIG. 6. Differential cross sections for $^{18}O(\pi,\pi')^{18}O(1^-, 4.46\ MeV)$ at 164 MeV. The curves at left and right, respectively, were calculated with ARPIN using the bare shell model densities and the enhanced densities shown in Fig. 7.

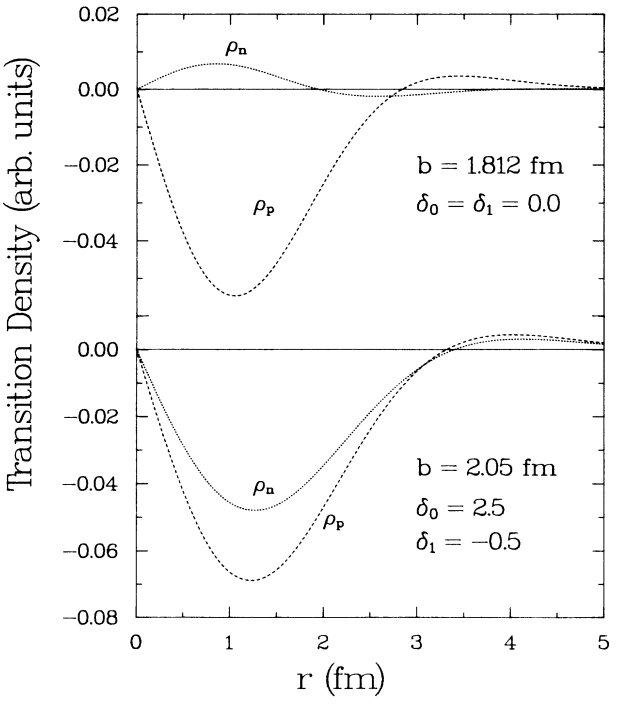

FIG. 7. Radial transition density for the 0^+-1^- transition. Top: Bare shell model prediction with $b'=1.812$ fm. Bottom: Enhanced transition density which fits (e,e') and $(\pi^{\pm},\pi^{\pm'})$ with $b=2.05$ fm.

good agreement with experiment. Use of the $(0+2)\hbar\omega$ wave functions for the positive parity states and the mixed 1^- state wave functions gives a further 15% increase in the predicted π^+ cross sections and leaves the π^- cross sections essentially unchanged. The effective charges required to fit the (e,e') and (π,π') data are only $\delta_0=\delta_1\simeq 0.7$ with the large value of $b=2.05$ fm, which is still needed to fit the shapes of the (e,e') form factor and the (π,π') angular distributions. Data[36,37] on the $M1$ decays of the 1_1^-; $T=1$ and 1_2^-; $T=1$ states of ^{18}F to the 0_1^-; $T=0$ level, for which the model wave function should be adequate, indicate a similar need to mix at least the first two 1^-; $T=1$ model states.[35]

To obtain the shape of the longitudinal form factor for the 4.46 MeV level using an oscillator parameter of about 1.8 fm, which is close to the values needed to fit form factors for other levels, it is necessary to introduce a $y^{5/2}$ term in the shell model form factor in addition to the $y^{3/2}$ power which arises from $p\rightarrow(sd)$ excitations; thus,

$$F_L \rightarrow y^{3/2}(1-\alpha y)e^{-y} . \tag{12}$$

The $y^{5/2}$ terms in Eq. (12) can arise from small $p\rightarrow sdg$ or $sd\rightarrow pf$ amplitudes, but it remains to be seen whether expanded shell model calculations will generate such terms of sufficiently large magnitude to fit the data. (We have already noted that a small improvement to the shape, but not the magnitude, can be achieved through the use of more realistic, i.e., Woods-Saxon, single particle wave functions.) For $b'=1.812$ fm and $\alpha=0.23$ Eq. (12) gives

an excellent fit to the form factor at 90°. Apparently, the destructive interference between the $y^{3/2}$ and $y^{5/2}$ terms generates the good agreement with the data when a realistic value for b' is used. When $b=2.05$ fm and $\alpha=0.093$, the fit in terms of χ^2 is considerably worse. Unfortunately, such fits provide us with a proton density only. Evidence that the neutron density is similar in shape to the proton density is provided by our fits to the inelastic pion scattering cross sections.

Since electron and pion data are fitted with the same empirical transition density and since CC effects are small in (e,e'), the good fit to the pion data suggests that CC effects would also be unimportant for (π,π') scattering to the 1^- state. However, the fit to the pion data may be accidental or may indeed be very poor once CC effects are included. Thus it is important to assess the effect of channel coupling before claiming that there exist shortcomings in the shell model calculations. In the following section we present the results of (π,π') CC calculations involving the coupling of the lowest 0^+, 2^+, 3^-, and 1^- states.

IV. COUPLED-CHANNEL CALCULATIONS

A. General remarks

The coupled-channels (CC) calculations presented in this section were performed in momentum space using a model[16] which is a direct extension of one frequently used to study intermediate energy pion-nucleus elastic[23] and inelastic[1] scattering. A momentum-space formulation of the problem is particularly suitable for adequately treating the nonlocal (p-wave dominated) pion-nucleon interaction at energies near the [3,3] resonance. In the coupled-channel model the pion-nucleus scattering matrix is obtained by solving sets of multichannel Lippmann-Schwinger equations of the form

$$T_{ab}=U_{ab}+\sum_m U_{am}G_m T_{mb} \tag{13}$$

for each total angular momentum $\mathscr{J}=\mathbf{l}_a+\mathbf{J}_a$ and total isospin $\tau=\mathbf{t}_\pi+\mathbf{T}_a$. Here, a, b, m, etc. label the various pion-nucleus states included in the model space, e.g., $a=(k_a l_a J_a T_a)$, where k_a is the pion-nucleus relative momentum in the pi-nucleus c.m. frame, l_a is the pion-nucleus relative orbital angular momentum, J_a, T_a are the nuclear spin and isospin, respectively. $\mathbf{t}_\pi$ is the isospin of the pion. The summation denotes a sum over discrete labels l_m, J_m, T_m and integration over momentum k_m. U_{ab} is the interaction potential and G_m is the propagator with outgoing wave boundary conditions. The set of integral equations [Eq. (13)] is solved numerically by standard matrix inversion techniques[23] and the on-shell pion-nucleus scattering matrix elements T_{fi} for the various excited final nuclear states are obtained.

In the CC calculations presented in this section, the interaction potential was constructed[1] from the pion-nucleon scattering amplitude and the lowest order nuclear density discussed in Sec. III A. The diagonal part of the interaction is the elastic optical potential, which was generated by the elastic pion scattering code PIPIT.[23] The same Gaussian cutoff parameter and the energy shift in the pion-nucleon collision energy as in the elastic optical potential were used in constructing the inelastic transition potentials. In all the CC calculations, two-way couplings were used between pairs of nuclear states.

The CC calculations involving the 1^- (4.46 MeV) state are divided into two classes: (1) three-state calculations, in which one collective state (2^+ or 3^-) is included in the coupling scheme along with the ground state of ^{18}O and the 1^- state, and (2) four-state calculations, with the 2^+ and the 3^- states both included. In both cases we determined separately the contributions of multistep processes to the 1^- excitation, both with and without the direct coupling between the 0^+ and the 1^- states. Our objective was to find out whether the interference between the direct and multistep excitation mechanisms would have large effects on the cross sections for the $0^+\rightarrow 1^-$ excitation. In addition, we performed two-state CC calculations including the ground state and one collective state (2^+ or 3^-) in order to estimate the effect of channel coupling on these strong excitations.

B. CC calculations without direct $0^+\rightarrow 1^-$ coupling

In the first set of calculations we determined the CC effects for the $0^+\rightarrow 1^-$ transition arising from couplings with either the 2^+ or the 3^- strongly collective states, or both, without the direct excitation of the 1^-.

The enhancement factors and the oscillator parameters deduced in Sec. III B, were used in the coupling of the 2^+ and the 3^- states with the ground state. In the absence of experimentally measured electromagnetic transition rates between the 1^- and the 2^+ states and between the 1^- and the 3^- states, we relied on the shell model predictions for these transitions. Because the $E3$ ($E2$) components are expected to dominate, only these matrix elements predicted by the shell model were used for the 1^--2^+ (1^--3^-) coupling with the same enhancement factors and oscillator parameters as for excitations of the corresponding multipolarity from the ground state. To fit the electron scattering data and the π^-/π^+ cross section ratio for the 2^+ excitation, polarization charges $\delta_0=1.5$ and $\delta_1=0$ were introduced, along with an oscillator parameter $b=1.70$ fm. A similar procedure for the 3^- excitation led to a pure isoscalar enhancement, $\delta_0=0.8$ and $\delta_1=-1.0$, with $b=1.80$ fm. For the 3^- excitation in ^{17}O, however, $B(E3)$ is fitted[4] by effective charges $\delta_0=1.2$ and $\delta_1=0$ with $b=1.63$ fm. We performed (0^+-2^+-1^-) calculations using both sets of $E3$ enhancement factors for the 2^+-1^- transition, as well as one without any enhancement. It was found that increasing the strength of the coupling in the second step causes an overall enhancement of the angular distributions without any change in shape. Comparison with experimental data (Fig. 8) shows that the angular distributions from purely two-step processes are out of phase with the data and, for the largest $E3$ enhancement, the magnitude near the first peak is too small by a factor of 40 (12) for π^+ (π^-). The shapes of the angular distributions from the (0^+-3^--1^-) calculations (Fig. 9) are similar, but the magnitudes larger than for the (0^+-2^+-1^-) calculations.

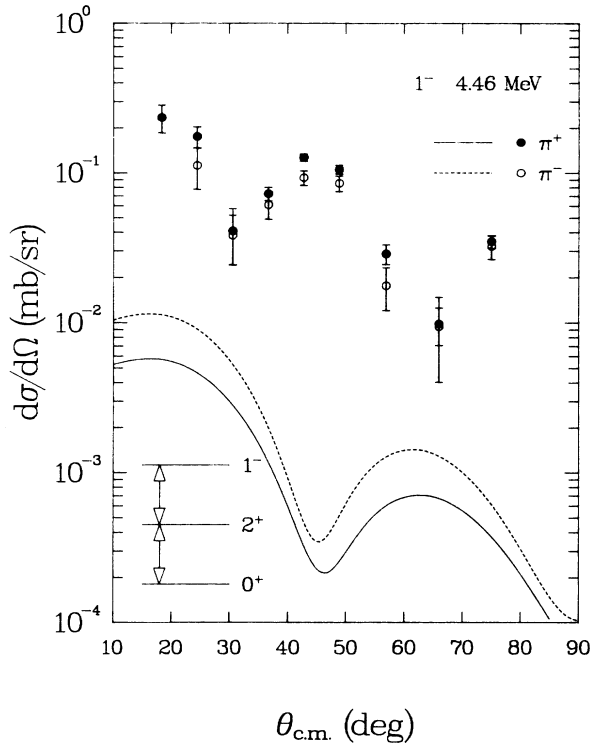

FIG. 8. Differential cross sections for $^{18}O(\pi,\pi')^{18}O(1^-, 4.46$ MeV) at $T_\pi = 164$ MeV obtained from three-state (0^+-2^+-1^-) CC calculations without 0^+-1^- direct coupling.

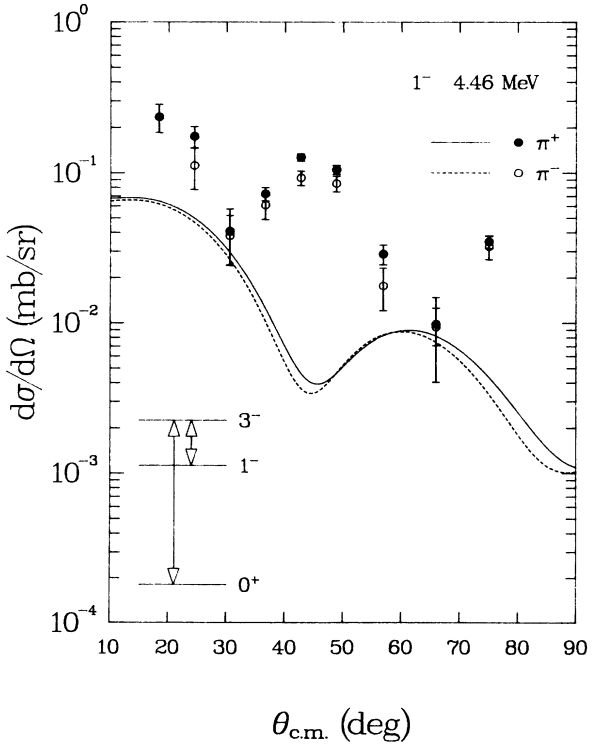

FIG. 9. Same as Fig. 8, but for (0^+-3^--1^-) coupling.

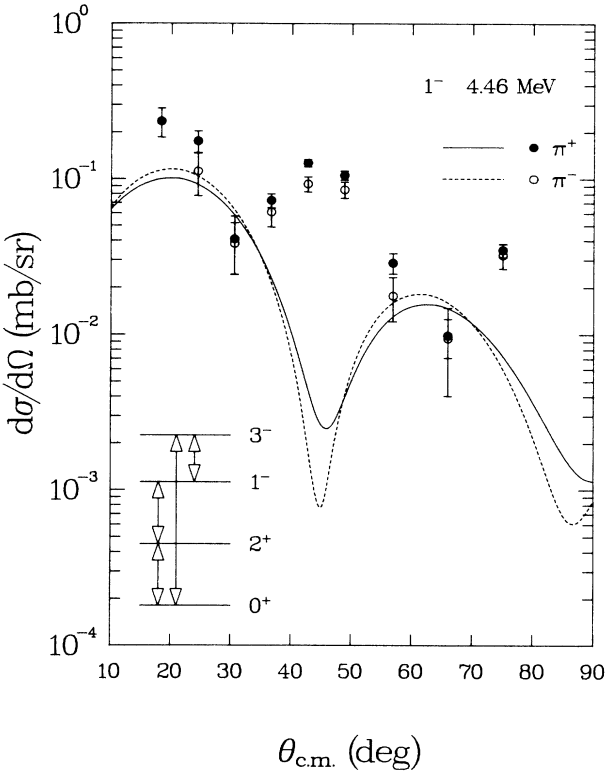

FIG. 10. Differential cross sections for $^{18}O(\pi,\pi')^{18}O(1^-, 4.46$ MeV) obtained from four-state (0^+-2^+-3^--1^-) CC calculations without 0^+-1^- direct coupling.

We also performed CC calculations including both the 2^+ and the 3^- states in the coupling scheme (Fig. 10). For these cases, once again the largest enhancement was used for the $E3$ coupling between the 1^- and 2^+ states. By comparing the theoretical curves in Figs. 8—10, it is seen that the qualitative features of the CC angular distributions are similar in all three schemes: the cross sections are out of phase with the data and too small. We note that multistep processes involving the 3^- state are more important than those involving the 2^+ state. In the next sections we examine the interference between the two-step and the direct 0^+-1^- couplings.

C. Three- and four-state couplings with unenhanced 1^- transition density

Calculations were performed which include the direct coupling between the 0^+ and the 1^- states using the bare 0^+-1^- coupling obtained from the shell model calculations (i.e., without enhancements) and $b = 1.812$ fm. For the case of coupling the $2^\pm$ intermediate state, we found that the shape of the angular distribution for the 1^- state is determined mainly by the direct coupling to the 1^- state and changes little when different $E3$ enhancements in the 1^--2^+ coupling are used. Consequently, in all the calculations that follow we decided to use the $E3$ enhancement obtained from the fit to the electron scattering data for the 0_1^+ to 3_1^- transition, i.e., $\delta_0 = 0.8$,

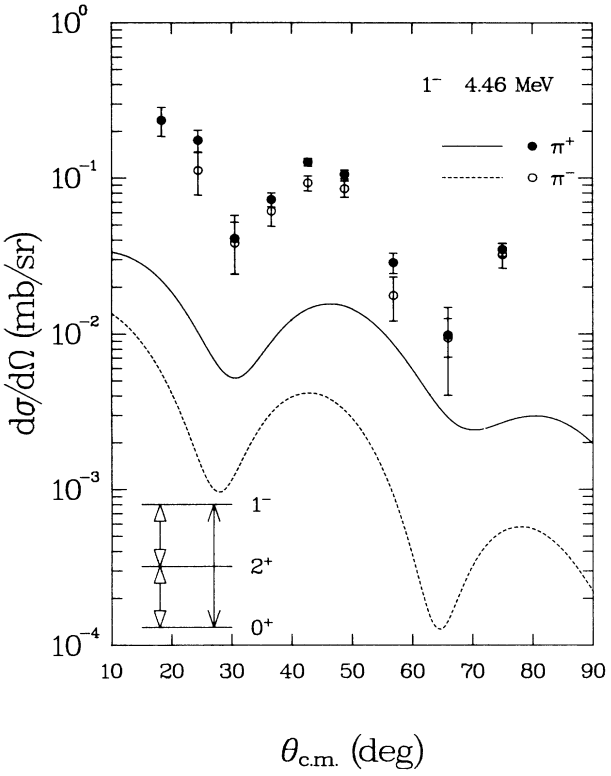

FIG. 11. Same as Fig. 8, but *with* the bare 0^+-1^- direct coupling.

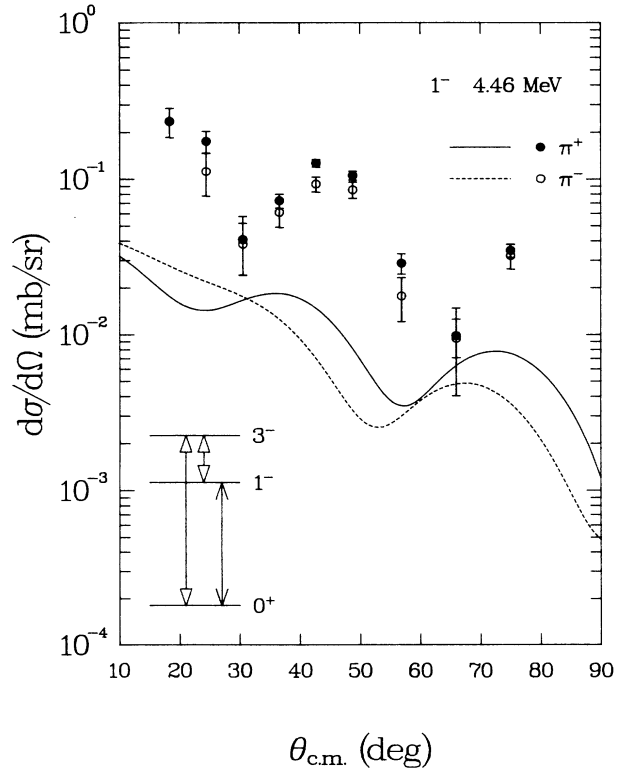

FIG. 12. Same as Fig. 8, but for (0^+-3^--1^-) and *with* the bare 0^+-1^- direct coupling.

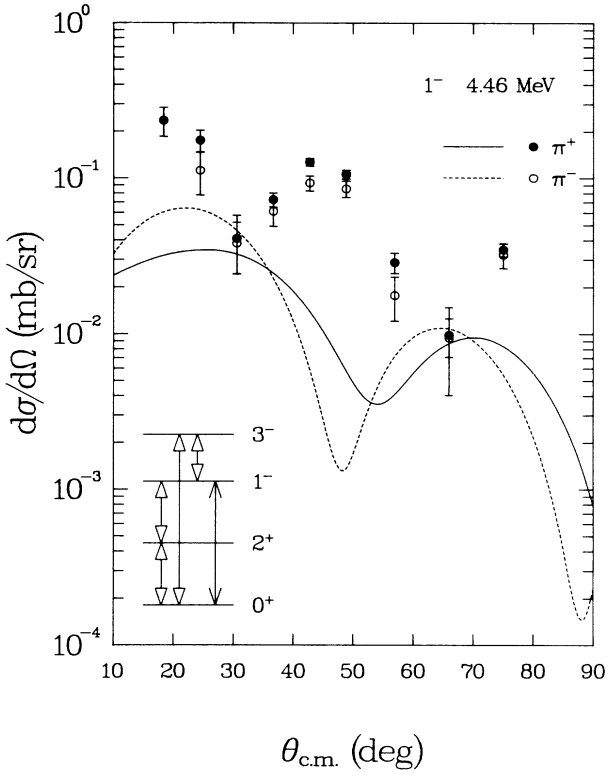

FIG. 13. Same as Fig. 10, but *with* the bare 0^+-1^- direct coupling.

$\delta_1 = -1.0$, and $b = 1.80$ fm.

Figures 11–13 show the angular distributions obtained from the 1^- state using three different coupling schemes (see insets of figures). The following observation can be made: Two-step processes involving the 2^+ state together with the direct 0^+-1^- coupling produce an overall enhancement of the 1^- angular distribution and an inward shift in the position of the minimum which brings it in phase with the data (Fig. 11). The enhancement is considerably larger for π^+ than for π^-, but the calculated cross sections are still much too small. Figure 12 shows the effect of including the 3^- state with the 0^+-1^- levels. The shape of the 1^- angular distribution is not reproduced and the absolute cross sections are also too small. If both the 2^+ and 3^- states are included with the direct $0^+ \rightarrow 1^-$ excitation (Fig. 13), the theoretical curves are completely out of phase with the data. It is clear that interference of two-step processes with the direct, unenhanced 0^+-1^- coupling does not generate agreement with the data.

D. CC calculations with enhanced 1^- transition density

CC calculations were also performed with the enhanced 1^- transition density discussed in Sec. III. Our objective was to determine the effect which channel coupling has on the excellent fit to the 1^- data [Fig. 6(b)] produced by DWIA calculations using the enhanced transition density

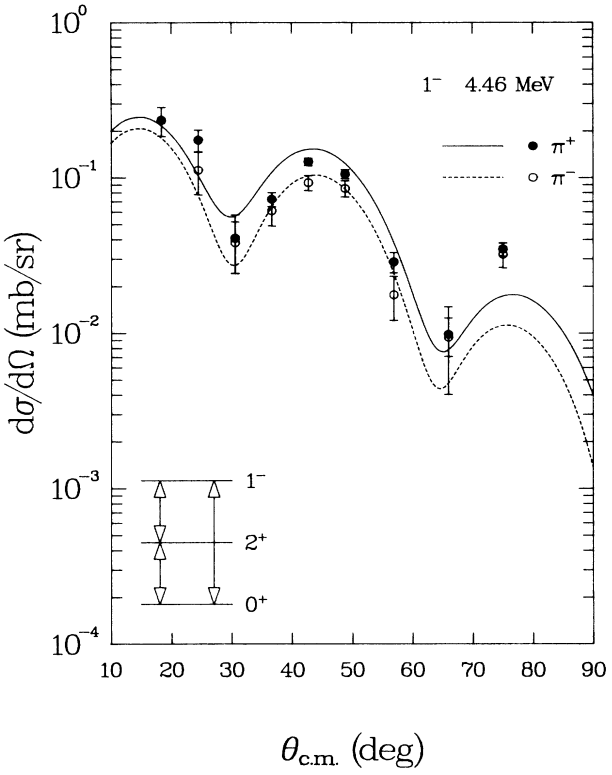

FIG. 14. Same as Fig. 8, but with the enhanced 0^+-1^- direct coupling.

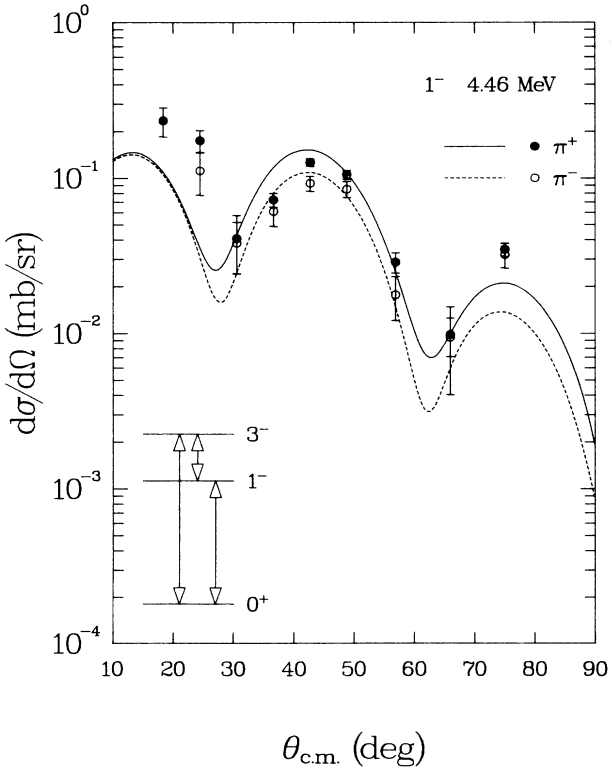

FIG. 15. Same as Fig. 8, but for $(0^+$-3^--$1^-)$ and with the enhanced 0^+-1^- direct coupling.

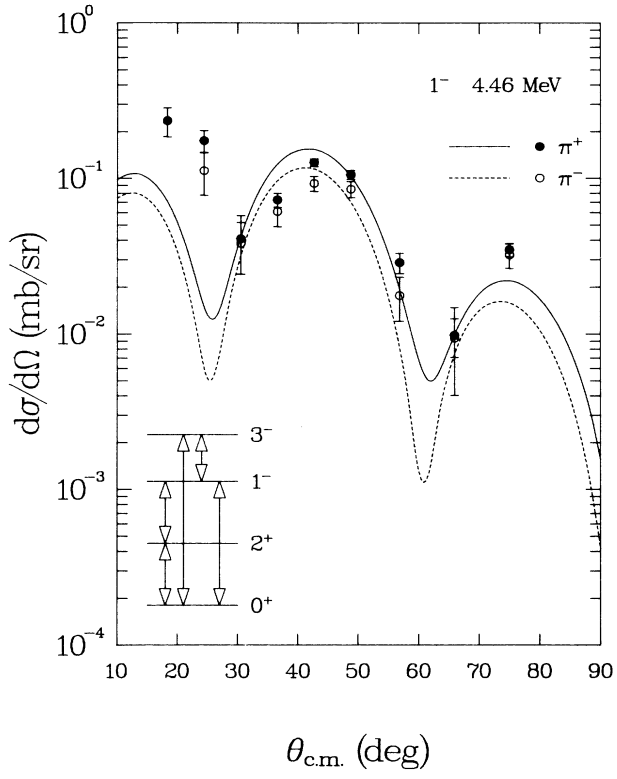

FIG. 16. Same as Fig. 10, but with the enhanced 0^+-1^- direct coupling.

(Fig. 7). Angular distributions for the 1^- state obtained from three- and four-state calculations are shown in Figs. 14—16. We found that the effect of channel coupling was to reduce the differential cross sections at the far forward angles ($\theta_{c.m.} < 30°$) and enhance them at large angles ($\theta > 60°$), while essentially preserving the good fit to the second peak. This was observed for all three coupling schemes, but was most pronounced for the four-state calculations and least for the $(0^+$-2^+-$1^-)$ three-state coupling.

E. Channel coupling effects on the collective 2^+ and 3^- states and the elastic scattering

To complete the study of channel coupling effects on the low lying states in ^{18}O, we calculated angular distributions for the 2^+ and 3^- states within the CC model using the coupling schemes discussed above. In addition, two-state calculations were carried out to determine the effect of channel coupling from the ground state alone. We found that the strongly excited collective states are affected mainly by coupling with the ground state, with negligible effects arising from multistep processes via the 1^- state, even when enhanced transition densities are used in all couplings. The results of two-state CC calculations for the 2^+ and the 3^- state are compared in Figs. 3 and 4, respectively, with the corresponding DWIA results using the same enhanced transition densities (see Secs. III B 2

and III B 3). We found that channel coupling enhances the 2^+ cross sections over DWIA results by 10% (7%) for π^+ (π^-). The effect is stronger for the 3^- state, where enhancement due to CC effects was found to be 19% (16%) for π^+ (π^-) at the peak cross section, thereby improving the agreement with data.

We note that channel coupling also affects the elastic scattering. At 180°, CC effects due to the 2^+ and 3^- states increase the π^- differential cross sections by about 35% (Fig. 3, dotted line). For π^+ (not shown) the increase is only 20%.

V. SUMMARY

We have analyzed differential cross sections for π^+ and π^- scattering from ^{18}O with particular emphasis on understanding the singularly poor fits of DWIA calculations for the 1^- state at 4.46 MeV. DWIA and CC calculations were done using a consistent set of shell model one body density matrix elements among the lowest 0^+, 2^+, 3^-, and 1^- states. Effective charge enhancement factors were deduced from electron scattering form factors, $B(E\,\Delta L)$ transition rates, and the π^+/π^- cross section ratio.

For the collectively enhanced transition to the 2^+ (1.98 MeV) state, the polarization charges are consistent with commonly used values and CC effects were found to be relatively minor. For the 3^- (5.09 MeV) state the shell model isovector transition density had to be quenched in order to fit the π^+/π^- ratio. Then the DWIA absolute cross sections are too small, but CC effects generate somewhat better agreement with the data.

For the 1^- state (4.46 MeV), the shell model wave functions provide poor fits to the (e,e′) data and fail in predicting the (π,π') cross sections whether multistep couplings are included or not. If the three lowest 1^- shell-model states are mixed in a manner suggested by the need to fit other data, such as nucleon pickup, the $p \rightarrow sd$ proton and neutron densities for the lowest level are enhanced. However, the longitudinal form factor still peaks at too large a momentum transfer and the DWIA cross sections for (π,π') are still a factor of the 4 too small. Therefore contributions from outside the $0\hbar\omega$ and $1\hbar\omega$ shell-model spaces are required to reproduce the shapes and magnitudes of the inelastic scattering cross sections for the 1^- state with a realistic value for b. Semiphenomenological proton and neutron transition densities were derived for the transition to the 1^- state. At $r > 3$ fm, the neutron density is quite large and in phase with the proton density, in contrast to the shell model prediction. These densities fit the (e,e′) and (π,π') data very well. CC effects are relatively more important for this transition, but the cross sections are nevertheless dominated by the direct 0^+-1^- coupling.

ACKNOWLEDGMENTS

The authors are indebted to Professor L. C. Bland, Professor P. J. Ellis, and Professor H. T. Fortune for valuable discussions. We thank Professor D. M. Manley and collaborators for permission to present their electron data prior to publication. A generous grant for computing time from the Supercomputer Institute at the University of Minnesota is gratefully acknowledged. This work was supported in part by the U.S. Department of Energy.

APPENDIX

The relationship between the OBDME's in *jj* and SU3 coupling is given by

$$\langle J_f T_f \| \|(a^\dagger_{j_1}\tilde{a}_{j_2})^{\Delta J \Delta T}\| \|J_i T_i\rangle = \sum_{(\lambda\mu)\kappa\Delta L\,\Delta S} (-1)^{Q_2} \langle (Q_1 0) l_1 (0\overline{Q}_2) l_2 \| (\lambda\mu)\kappa\Delta L\rangle \times \begin{Bmatrix} l_1 & \frac{1}{2} & j_1 \\ l_2 & \frac{1}{2} & j_2 \\ \Delta L & \Delta S & \Delta J \end{Bmatrix} \langle J_f T_f \| \|(a^\dagger_{(Q_1 0)}\tilde{a}_{(0Q_2)})^{(\lambda\mu)\kappa\Delta L\,\Delta S}\| \|J_i T_i\rangle \,. \tag{A1}$$

The definition of the reduced matrix element is that of Brink and Satchler.[30] The unitary $9J$ symbol is equal to the $9J$ symbol of Brink and Satchler multiplied by $\hat{j}_1\hat{j}_2\,\Delta\hat{L}\,\Delta\hat{S}$, where $\hat{j} = \sqrt{2j+1}$. $Q = 2n + l$ is the number of oscillator quanta. The SU3 ⊃ R3 Clebsch-Gordan coefficient is that of Draayer and Akiyama[38,39] and the bar over an SU(3) representation label corresponds to the case $(IJ) = (10)$ in Table I of Ref. 38; $(IJ) = (01)$ otherwise. With the correspondences $a^\dagger$ to $b^\dagger$, $\tilde{a}$ to $h^\dagger$, the *jj* and *LS* OBDME's of this work are identical in definition to those of Lee and Kurath[1] apart from an additional factor i^l in the definition of the single particle wave functions used here. The inverse of Eq. (A1) involves a straightforward sum over $l_1 l_2 j_1 j_2$.

For *p* to *sd* transitions ($Q_2 = 1$, $Q_1 = 2$) the SU3 ⊃ R3 coefficients take the values $\sqrt{1/6}$, $-\sqrt{5/6}$, $\sqrt{5/6}$, $\sqrt{1/6}$, -1, and 1 for $l_1(\lambda\mu)\Delta L$ equal to 0(10)1, 2(10)1, 0(21)1, 2(21)1, 2(21)2, and 2(21)3, respectively.

*On leave from the Department of Physics, Jadavpur University, Calcutta 700032, India.
†Present address: Los Alamos National Laboratory, P-Division, Los Alamos, NM 87545.
‡Present address: Mission Research Corporation, Santa Barbara, CA 93102.

[1]T.-S. H. Lee and D. Kurath, Phys. Rev. C **21**, 293 (1980); C **22**, 1670 (1980).
[2]T.-S. H. Lee and R. D. Lawson, Phys. Rev. C **21**, 679 (1980).
[3]S. J. Seestrom-Morris *et al.*, Phys. Rev. C **26**, 594 (1982).
[4]C. L. Blilie *et al.*, Phys. Rev. C **30**, 1989 (1984).
[5]D. B. Holtkamp *et al.*, Phys. Rev. C **31**, 957 (1985).
[6]D. Dehnhard and S.J. Seestrom-Morris, in *Proceedings of the International Symposium on Electromagnetic Properties of Nuclei,* Tokyo, 1983, edited by H. Horie and H. Ohnuma (Tokyo Institute of Technology, Tokyo, 1983).
[7]D. J. Millener and D. Kurath, Nucl. Phys. **A255**, 315 (1975).
[8]P. J. Ellis and T. Engeland, Nucl. Phys. **A144**, 161 (1970); **A181**, 368 (1972), and private communication.
[9]E. Oset and D. Strottman, Phys. Lett. **84B**, 396 (1979).
[10]F. Petrovich, Phys. Rev. C **16**, 839 (1977).
[11]B. A. Brown *et al.*, Phys. Rev. C **26**, 2247 (1982).
[12]F. Ajzenberg-Selove, Nucl. Phys. **A392**, 1 (1983).
[13]S. J. Seestrom-Morris, D. B. Holtkamp, and W. B. Cottingame, in *Spin Excitations in Nuclei,* edited by F. Petrovich, G. E. Brown, G. T. Garvey, C. D. Goodman, R. A. Lindgren, and W. G. Love (Plenum, New York, 1984).
[14]M. Gai, M. Ruscev, A. C. Hayes, J. F. Ennis, R. Keddy, E. C. Scholemer, S. M. Sterbenz, and D. A. Bromley, Phys. Rev. Lett. **50**, 239 (1983), and private communication.
[15]M. Gmitro, J. Kvasil, and R. Mach, Phys. Rev. C **31**, 1349 (1985).
[16]S. Chakravarti, Phys. Lett. **90B**, 350 (1980).
[17]C. L. Morris *et al.*, Phys. Rev. C **30**, 662 (1984).
[18]D. J. Millener, J. W. Olness, E. K. Warburton, and S. S. Hanna, Phys. Rev. C **28**, 497 (1983).
[19]H. A. Thieseen and S. Sobottka, Los Alamos National Laboratory Report LA-4534-MS, 1970 (unpublished).
[20]G. Rowe, M. Salomon, and R. H. Landau, Phys. Rev. C **18**, 584 (1978).
[21]S. J. Seestrom-Morris *et al.*, Phys. Rev. C (in press).
[22]S. Iversen *et al.*, Phys. Lett. **82B**, 51 (1979).
[23]R. A. Eisenstein and F. Tabakin, Comput. Phys. Commun. **12**, 237 (1976).
[24]B. E. Norum *et al.*, Phys. Rev. C **25**, 1778 (1982), and private communication.
[25]J. A. Carr, F. Petrovich, and J. Kelly, program ALLWORLD (modified by M. A. Franey) (unpublished).
[26]W. Chung, Ph.D. thesis, Michigan State University, 1976 (unpublished).
[27]D. Stanley and F. Petrovich, program ELEC (unpublished).
[28]G. C. Ball *et al.*, Nucl. Phys. **A377**, 268 (1982).
[29]A. C. Hayes, Ph.D. thesis, Yale University, 1986.
[30]D. M. Brink and G. R. Satchler, *Angular Momentum* (Clarendon, Oxford, 1968).
[31]J. L. Groh, R. P. Singhal, H. S. Caplan, and B. S. Dolbilkin, Can. J. Phys. **49**, 2743 (1971).
[32]D. M. Manley, B. L. Berman, W. Bertozzi, T. N. Buti, J. M. Finn, F. W. Hersman, C. E. Hyde-Wright, M. V. Hynes, J. J. Kelly, M. A. Kovash, S. Kowalski, R. W. Lourie, B. Murdock, B. E. Norum, B. Pugh, and C. P. Sargent (unpublished).
[33]T. N. Buti *et al.*, Phys. Rev. C **33**, 755 (1986).
[34]G. Th. Kaschl *et al.*, Nucl. Phys. **A155**, 417 (1970).
[35]A. C. Hayes, D. A. Bromley, and D. J. Millener (unpublished).
[36]I. Berka *et al.*, Nucl. Phys. **A288**, 317 (1977).
[37]J. C. Sens, S. M. Refaei, and A. Pape, Phys. Rev. C **18**, 2007 (1978).
[38]J. P. Draayer and Y. Akiyama, J. Math. Phys. **14**, 1904 (1973).
[39]Y. Akiyama and J. P. Draayer, Comput. Phys. Commun. **5**, 405 (1973).